BMC Cancer

RESEARCH

Open Access

Targeting cellular plasticity: esculetin-driven reversion of stem cell-like characteristics and EMT phenotype in transforming cells with sequential p53/p73 knockdowns

Ankit Mathur[1,2], Chanchal Bareja[2†], Milky Mittal[2†], Anjali Singh[2] and Daman Saluja[1,2*]

Abstract

The intricate interplay of cancer stem cell plasticity, along with the bidirectional transformation between epithelial-mesenchymal states, introduces further intricacy to offer insights into newer therapeutic approaches. Differentiation therapy, while successful in targeting leukemic stem cells, has shown limited overall success, with only a few promising instances. Using colon carcinoma cell strains with sequential p53/p73 knockdowns, our study underscores the association between p53/p73 and the maintenance of cellular plasticity. Morphological alterations corresponding with cell surface marker expressions, transcriptome analysis and functional assays were performed to access stemness and EMT (Epithelial-Mesenchymal Transition) characteristics in the spectrum of cells exhibiting sequential p53 and p73 knockdowns. Notably, our investigation explores the effectiveness of esculetin in reversing the shift from an epithelial to a mesenchymal phenotype, characterized by stem cell-like traits. Esculetin significantly induces enterocyte differentiation and promotes epithelial cell polarity by altering Wnt axes in Cancer Stem Cell-like cells characterized by high mesenchymal features. These results align with our previous findings in leukemic blast cells, establishing esculetin as an effective differentiating agent in both Acute Myeloid Leukemia (AML) and solid tumor cells.

Keywords Esculetin, Cancer stem cells, p53, p73, HCT116, Differentiation, Wnt signalling

Introduction

In the context of carcinogenesis, the acquisition of a spectrum of phenotypic identity is essential for the growth and dissemination of cancer cells. Moreover, cellular plasticity is integrally associated with the emergence of intra-tumoral heterogeneity and therapy response. Such phenotypic switching has extensively been studied [1, 2] during early invasive events in solid tumours widely known as Epithelial-Mesenchymal Transition (EMT). Recent evidence has indicated that a small subset of undifferentiated cells within the heterogenous population exhibit distinct features of stem cells (CSCs) as well as elevated EMT programming

†Chanchal Bareja and Milky Mittal contributed equally to this work and share second authorship.

*Correspondence:
Daman Saluja
dsalujach1959@gmail.com; dsalujach59@gmail.com
[1]Delhi School of Public Health, Institution of Eminence, University of Delhi, Delhi 110007, India
[2]Dr. B.R. Ambedkar Center for Biomedical Research, University of Delhi, Delhi 110007, India

which function in complement to evade the cells from the primary site. Given their distinctive ability for self-renewal as well as differentiation potential, CSCs have gained attention as a better model to represent the highly dynamic nature of cancer initiation, promotion, progression, and relapse [3]. Furthermore, the ability of CSCs to modulate their phenotype to escape the conventional therapeutic regimes instigates the development of innovative approaches to specifically target CSC [4]. Studies have suggested that irrespective of the type of malignancy, targeting CSC plasticity promises more precise therapeutic rationales for anti-cancer therapeutics [5]. One of the successful examples of hijacking the CSC plasticity is development of treatment regimens that remove maturation block and promote differentiation in leukemic stem cells that resulted in remarkable cure rates in some of the Acute Myeloid Leukemia (AML) subtypes [6]. Despite substantial efforts to imply the similar therapeutic strategy on other tumour types, at present a handful of evidences promises successful applicability of differentiation therapy on solid tumours. In this regard, identification of novel therapeutic agents and a deeper understanding of the mechanism of CSC differentiation might help in improving the cellular reprogramming technology in solid tumours as well. We have previously shown that a natural compound, Esculetin (Es) profoundly induce antiproliferative effects in AML as well as in pancreatic cancer cell lines [7, 8]. More recently, we reported the potential of esculetin to release the maturation arrest and induce neutrophilic differentiation in leukemic blast cells [8]. Our study also highlights the "axis shift" of Wnt signaling during esculetin-mediated blast cell differentiation. Therefore, we aspire to investigate any possible role of esculetin on the plasticity of solid tumour cells undergoing EMT. Considering that the reciprocal relationship between EMT and CSCs attributed by one or more genetic hit in the key tumour suppressor/oncogenic genes, we used a cellular model of HCT116 colon carcinoma cells with sequential knockdown of the well-known tumour suppressor genes p53 and its family protein p73. Interestingly, this attractive model was found to be a working cellular model for evaluating effect of esculetin, if any, on the plastic nature of CSCs undergoing EMT.

Materials and methods

Cell culture and maintenance of cell lines

HCT116 WT and HCT116p53$^{-/-}$ p73$^{+/+}$ cell lines were obtained from Bret Vogelstein lab, John Hopkins University, Mayerland, US. The HCT116p53$^{-/-}$p73kd strain was generated as described earlier [9]. Briefly, TAp73 targeted shRNA was cloned in pBABEU6 vector. Lipofectamine 2000 (Invitrogen) was used for transfection and puromycin resistant clones were selected. Sequences used for TAp73 shRNA: TAp73 (5′ - GGCATGACTAC ATCA −3′), scrambled for TAp73 (5′ - GCCAGACTC GTTTACATGA −3′). All three strains were maintained in Dulbecco's Modified Eagle Medium (DMEM/Invitrogen) supplemented with 10% fetal bovine serum, Penicillin-50,000 Units/L and Streptomycin- 50 µg/ml at 37^{0}C in a humidifier incubator.

Treatment with Esculetin: Esculetin (6,7-dihydroxycoumarin/cichorigenin) is a coumarin derivative with hydroxyl groups at positions 6 and 7 on the benzopyrone core was purchased from Sigma-Aldrich (Cat. No. Y0001611; Purity: 98%). Esculetin was dissolved in DMSO and diluted appropriately to achieve a final DMSO concentration of 0.04%. The final concentration of esculetin was adjusted as specified in the experimental protocol.

Western blotting

Cells were lysed in a buffer containing 2% SDS, 20% glycerol, and 50 mM Tris-HCl along with a protease inhibitor cocktail (Sigma, USA) at 4 °C for 1 h. Laemmli buffer was added, and the samples were boiled for 10 min to denature the proteins. The protein lysates were then subjected to 10% SDS-PAGE for separation. The separated proteins were subsequently transferred onto a methanol-pretreated PVDF (Polyvinylidene fluoride) membrane. Protein expressions were assessed using western blotting. Anti-E cadherin (abcam; ab40772), anti-N-cadherin antibody (Dilution 1:1000; abcam; ab7601), anti-vimentin (Dilution 1:1000; abcam; ab76011), anti-phospho-β-catenin antibody (Dilution 1:1000; abcam; ab53050) and anti-β Actin (Dilution 1:500; Santa Cruz Biotechnology; sc-1615) antibodies were used. Protein bands were detected using chemiluminescence detection system (Bio-Rad) and quantification was carried out using ImageQuant system (GE Healthcare).

Cell viability analysis by MTT Assay

MTT assay detects the cell viability by measuring the reduction of (3-(4,5-dimethylthiazolyl-2)-2,5-diphenyltetrazolium bromide) by mitochondrial succinate dehydrogenase in metabolically active live cells. HCT116 strains (25×10^4 cells/well) were seeded in 96 well plates and then exposed to varied concentrations of esculetin following 24 h post-seeding. Following the exposure, cells were incubated with MTT for 3 h and crystals were dissolved in DMSO and absorbance at 570 nm was measured using Tecan spark control software.

Cell proliferation analysis by growth kinetics

Cell proliferation was analysed by growth kinetics assay at different time intervals with and without esculetin (100 µM) treatment. Briefly, 30,000 cells were seeded in

35 mm Petridishes. Subsequently cells were counted at different time intervals of 24 h up to 96 h using Neubauer hemocytometer.

Cell cycle analysis

Cell cycle distribution of esculetin treated/untreated cells at varied time intervals was measured using Propedium Iodide (PI) method. Cells were fixed in 70% chilled ethanol overnight and washed with PBS. Cells were then incubated at 37^0 C for 30 min after adding RNAse A (100 µg/ml). Propidium Iodide (10 µg/ml) was incorporated directly 15 min before acquisition by FACS Calibur (BD Biosciences).

Wound healing (Migration Assay) assay

Wound healing assay was performed to study cell migratory potential of esculetin treated/untreated cells. Briefly a monolayer of HCT116 cells were scratched with 200 µl micro-pipette tip and treated with 100µM esculetin. We employed a reduced serum concentration (5%) throughout the process to suppress cell proliferation and ensure the exclusion of duplicating cells. Images were captured at different random areas immediately or 18 h after scraping under NIKON TI2 microscope and distance travelled by cells was measured by calculating the distance between the two-leading edge of the wound.

Anchorage independency by soft agar colony assay

Soft agar assay was performed as described previously [10]. Briefly, 50,000 cells/60 mm Petridish were embedded in 0.33% agarose overlaid on a 2% agarose layer and covered with fresh growth medium. Colony growth was analysed after two weeks under NIKON TI2 microscope.

Anoikis resistance

Anoikis Resistance was analysed by seeding 8×10^4 cells in suspension on polystyrene Petridishes (Non-tissue culture treated; Tarsons). Following 48 h esculetin treatment, floating live vs. dead cells were detected and counted using Tryphan blue (K940, Amresco, Dallas, Texas, United States) and Neubaur improved haemocytometer. Ratio of live/dead cells was indicative of anoikis resistance.

Flow cytometry

Cell size by flowcytometry was analysed by measuring the scatter characteristics of exponentially growing unfixed unstained cells using FACSaria flow cytometer (Becton Dickinson). 2-3$\times10^6$ cells resuspended in PBS was measured for relative changes in scatter properties reflecting the cell size (Forward Scatter) and granulation (Side Scatter).

For cell surface marker analysis, approximately 1×106 cells were resuspended in PBS containing 0.5% Bovine Serum Albumin (BSA) for 1 h to inhibit non- specific antibody binding. Cells were then stained with FITC-anti-CD24/Percp5.5-anti-CD44 and PE.cy7-anti-CD90 antibodies in combination and /alone (Biolegend). Stained cells were then analysed by FACS aria flowcytometer.

Quantitative real time PCR analysis

Primers were designed using NCBI PRIMER BLAST and PRIMER3 for the desired genes. Primer sequences are described in supplementary Table 1. An equal volume of cDNA was used for real time PCR using Quanti-Tect SYBR green PCR Kit (204143; Qiagen) as per the manufacturer's instructions. β-Actin was used as a loading control.

Bioinformatics approach to analyze stemness signatures

To investigate whether acquisition of EMT features upon p73 deletion is associated with stemness, we employed Transcriptome analysis of HCT 116 $p53^{-/-}$ $p73^{+/+}$ and $p53^{-/-}$ p73kd cells which was outsourced to Xcelris Labs Limited, Ahmedabad, Gujarat, India. Differentially expressed genes were obtained in both the sets. Log2FC>0; $p<0.05$ was used as a filter to sort significantly upregulated genes. Further, we utilized the stem cell checker database to see if these genes are involved in stemness signatures. StemChecker assesses the statistical significance of the overlap between the uploaded genes and those in curated stemness signatures. The stem cell checker database utilized Bonferroni correction to understand the association. This data was further clinically validated with a tissue expression dataset in NCBI- GEO. GSE44076 was sorted out which closely mimics our cellular model system. GEO2R was leveraged to identify DEGs and $p<0.05$ was used as a parameter of significance. Venny2.1 was used to find the common genes between the Transcriptome Stem cell pool and GSE 44,076.

Colonosphere formation

The colonospheres formation was carried out as described by Liu et al. [11], with slight modifications. Briefly, 6×10^4 cells per well were seeded in 2 ml stem cell media containing DMEM/F12 (1:1) supplemented with B27 (Gibco), 20 ng/ml Human EGF recombinant protein (Gibco), 10 ng/ml Human FGF-basic recombinant protein (Gibco), and pen-strap antibiotics in a 6-well ultra-low-attachment plates (Corning Inc, Lowell, MA). The colonospheres formed at the end of the incubation period were centrifuged (1000 rpm), dissociated with 0.25% trypsin/EDTA with gentle agitation at 37^0C to obtain single cell suspension.

Statistical analysis of data

Wherever necessary, differences in the mean (±SE) values of different treatments were analysed for significance using the unpaired two-tailed Student's t-test for independent samples.

Results

HCT116 cell strains with sequential knockdown of p53/p73 exhibit stable EMT characteristics and activated canonical wnt pathway

DIC microscopic evaluation of HCT116 WT and its transformants revealed a marked phenotypic alteration akin to epithelial to mesenchymal trans-differentiation. A distinct cobblestone like morphology was comparable to the epithelial phenotype of HCT116 WT cells that changed to relatively more elongated and spindle-shaped cells with an increase in length/breath ratio (up to two-fold) in the $p53^{-/-}$ $p73^{+/+}$and $p53^{-/-}$p73kd cell strains (Fig. 1A). One of the characteristics mesenchymal features i.e., tight and firm attachment to the surface was evaluated by the degree of attachment to the cell culture plastic plates [12, 13]. We found up to 60% increase in cell attachment area of HCT116$p53^{-/-}$ p73kd cells as compared to the wild type cells (Fig. 1B). Cell spreading or adherence to the surface could be partly influenced by the cell size. Therefore, scatter characteristics of unfixed, suspended cells were analyzed by flow cytometry. The cell size indicated by forward scatter was found to be unaltered among all the three cell strains confirming a higher inherent spreading capacity of $p53^{-/-}$/p73kd strain as compared to the parental strains (Supplementary Fig. 1).

During EMT, epithelial cells deconstruct apico-basal polarity to facilitate motile behavior driven by alterations in cell adhesion molecules. Analysis of the leading edges extending into the open area of the exponentially growing cultures revealed striking differences in cell movement of all the three cell strains. A tightly packed monolayer of wild type strain with smooth periphery had limited cell movement towards the empty spaces. Whereas, a preferential directional movement of cells with prominent filopodial protrusions were observed in the spatial organization of $p53^{-/-}$p73kd cells. On the other hand, an intermediate cell movement patterns were detected in the growing $p53^{-/-}$ $p73^{+/+}$ cells (Fig. 1C). These observations corresponded with up to two-fold increased cell migration in $p53^{-/-}$p73kd strain when analyzed by wound healing assay (Fig. 1D). The above functional characteristics corroborated with alteration in cell adhesion molecule expression profile. We observed downregulation of E-cadherin while more than two-fold upregulation of N-cadherin and vimentin expression in $p53^{-/-}$p73kd cells at both protein (Fig. 1E) as well as transcript levels (Fig. 1F). We also observed up to a two-fold increase in key EMT-associated transcription factors, including *SNAIL1*, *TWIST1*, and *ZEB2*, in the p73kd strain (Fig. 1G). The Wnt signaling pathway has been established to contribute to the trans-differentiation of one cell type to another. RNA-Seq differential expression analysis of $p53^{-/-}p73^{+/+}$ and $p53^{-/-}$p73kd cells revealed significantly altered Wnt-associated genes (Fig. 1H). Within the Wnt signaling pathway, we found upto ~ 25-fold upregulation of 10 activators (*DVL3*, *LRP1B*, *CTNND1*, *CTNNA1*, *CTNNBIP1*, *TCF7L2*, *TCF12*, *CDC42BPG*, *CCNC*, *HOXA1)* while downregulation of 7 suppressors (*KREMN2*, *KREMN2*, *CTBP2*, *AXIN2*, *PORCN*, *TLE3*, *LAT2*) of canonical Wnt pathway. However, genes associated with activation of non-canonical Wnt Ca^{2+} (*CAMKK2*, *RAC2*, *PLCB4*, *NFATC2*) were found to be downregulated. The prerequisite event in the activation of the canonical Wnt pathway is the stabilization of β-catenin through dephosphorylation. Incidentally, a significant downregulation of p-β-catenin protein was observed in $p53^{-/-}p73^{+/+}$ and $p53^{-/-}$p73kd cells as compared to the WT strain, thereby strongly indicating canonical Wnt axis activation in both the transformants, apparently having a higher mesenchymal characteristics (Fig. 1E/ lower panel).

Epithelial to mesenchymal conversion of HCT116 strains is associated with aggressive behavior

To determine whether the acquisition of mesenchymal features in $p53^{-/-}$p73kd cells accompany aggressive features, we checked anoikis (cell detachment mediated cell death) resistance of all the three strains. A marked tendency to spread upon the non-adherent hydrophobic surfaces was displayed by the wild-type cells while cell lines with p53-/-, p73+/+ while double knock out showed reduced efficiency to adhere (data not shown). Concurrently, ~ 30% reduction in floating dead cell of $p53^{-/-}$p73kd cells were observed, indicating the acquisition of anoikis resistance in HCT116p53-/- p73kd cells as compared to wild type cells (Fig. 2A). However, the size of the soft agar colonies remained unchanged across all strains suggesting that p53/p73 deletions could not accelerated the anchorage independency in the HCT116 cells (Fig. 2B).

Saturation density has been classically used as a measure of neoplastic progression [14, 15]. The acquired EMT phenotypes also correlated with considerably increased saturation densities (Fig. 2C) as well as accelerated growth potential in both the $p53^{-/-}$ and p73 knockdown strains at later time points (72 h onwards) as measured by growth kinetics assay (Fig. 2D).

EMT phenotype inherited with acquisition of stem cell-like characteristics in HCT116 colonospheres

To investigate any possible effect of p73 deletion on the stemness in cells displaying mesenchymal features, we

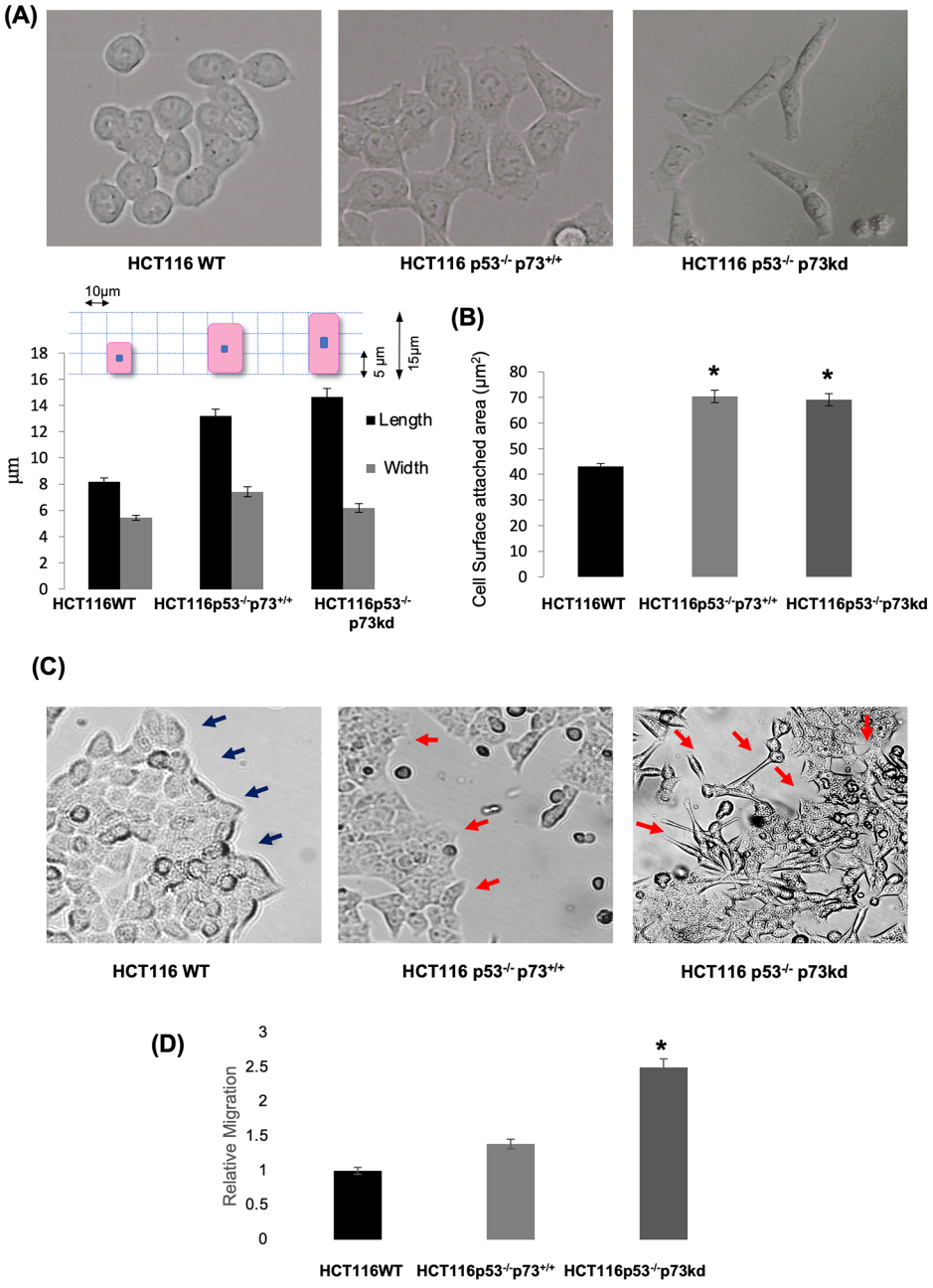

Fig. 1 Induction of EMT in HCT116 cell strain: (**A**) DIC microscopy images of HCT116 cells strain (magnification 40X) showing progressive phenotypic alterations. Cell length/breadth ratio was measured using NIS-elements-AR software. Phenotypic alterations reflect EMT phenotypes. (**B**) Area of surface attached cells to the tissue culture dishes were measured 48 h post seeding. Data represent the Mean ± SE of 50 cells measured in three independent experiments (*$p \leq 0.05$). (**C**) DIC images of exponentially growing culture (magnification 20X). (**D**) Wound healing analysis for cell migration 18 h after scraping. Cell migration was measured by the average distance (µm) travelled by cells from edges of scraped region towards the center. (**E**) Western blot analysis for EMT markers and p-β-Catenin expression. Cells were harvested for protein extraction at log phase of the culture. Histogram represents densitometric analysis of corresponding protein expression relative to β-actin expression (*$p \leq 0.05$) (Upper right panel). (**F**) qPCR analysis of EMT markers and (**G**) key transcription factors expression levels. β-actin was used as housekeeping control for normalization (*$p \leq 0.05$). (**H**) Transcriptome analysis of HCT116p53-/-p73+/+ and HCT116p53-/-p73kd reveals differentially regulated Wnt pathway components

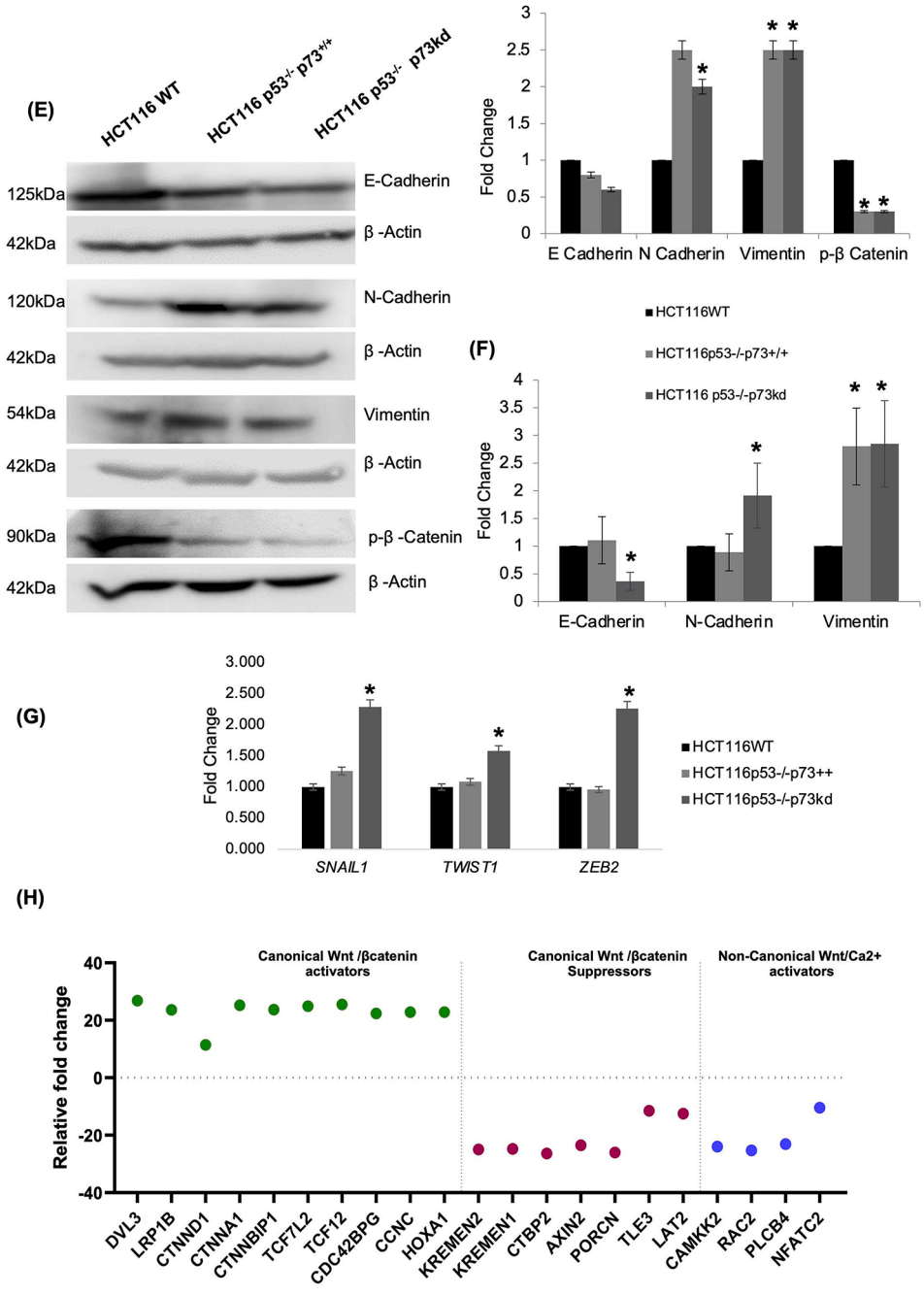

Fig. 1 Continued

employed transcriptome data of cell strains $p53^{-/-}p73^{+/+}$ and $p53^{-/-}$p73kd. In total, 1055 upregulated and 1494 downregulated genes were found to be significantly altered (p value < 0.05). We then utilized the StemChecker database to validate our set of genes with the inbuilt datasets of the StemChecker database. We observed 440/3029 embryonic stem cells while 135/969 hematopoietic stem cells related genes to be the maximumly overlapped genes with a significant p-value ($p < 0.05$) (Fig. 3A/Lower panel). Interestingly, 21% fractional overlap was observed in the embryonic stem cell (ESCs) pool, suggesting the acquisition of pluripotent features upon p73 knockdown. 20% of genes were found to be common in the embedded expression profiles in the database (Fig. 3B). Consistent with the above findings, expression profiles investigating embryonic stem cells were found to be enriched. Out of the analyzed expression profiles, significant overlap ($p < 0.05$) was observed in 5 stemness signature datasets. Approximately 9% of the genes exhibit a match with TF (Transcription Factor) target genes. Within this, both

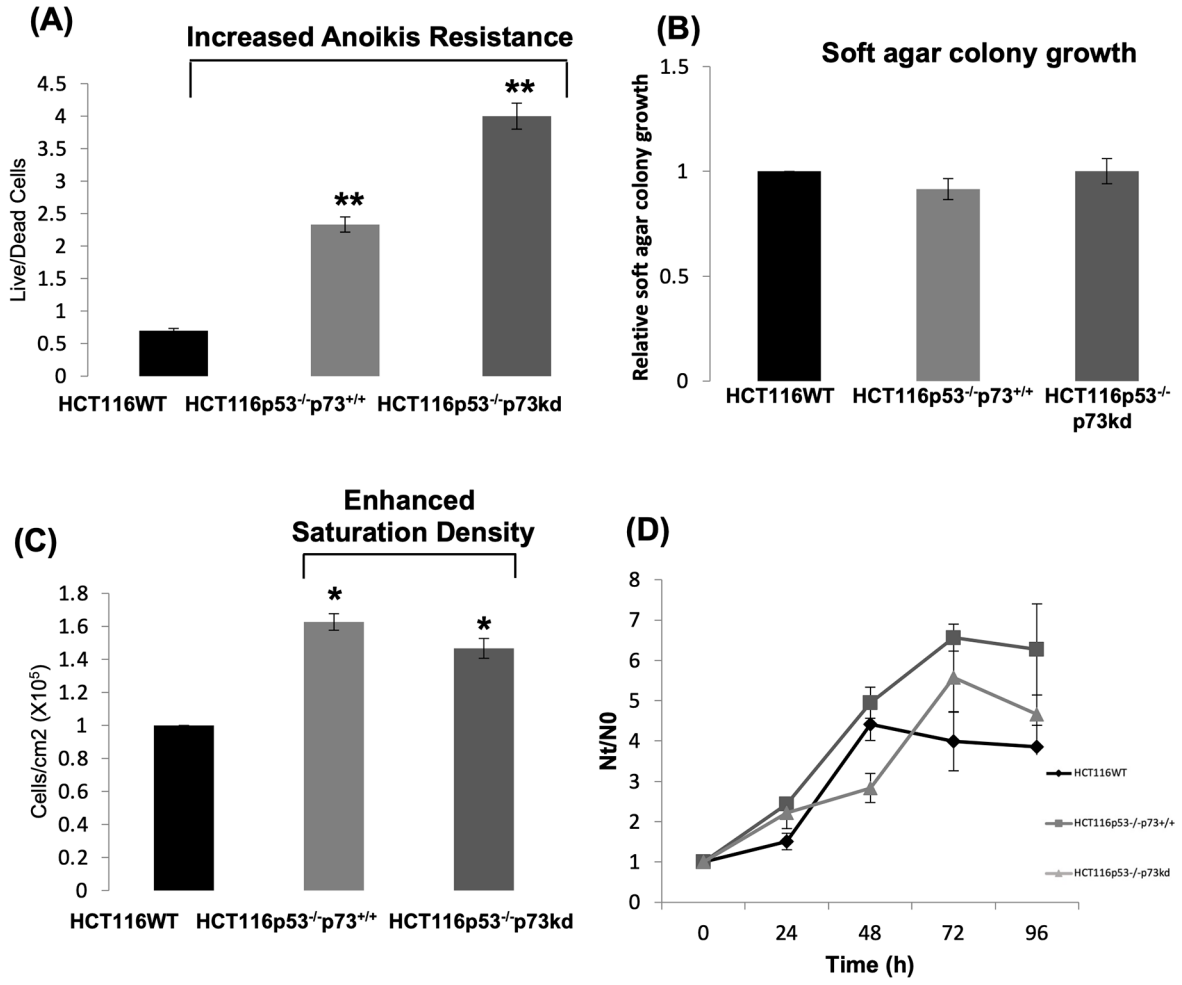

Fig. 2 Cell aggressiveness in HCT116 cell strains with sequential p53/p73 knockdowns: (**A**) Bar graph showing live/dead cells indicative of Anoikis Resistance which was measured by counting the floating live and dead cells using tryphan blue 48 h post seeding in polystyrene Petridish. (*$p \leq 0.05$ & **$p \leq 0.01$) (**B**) Soft agar colony formation assay to measure anchorage independent growth in HCT116 cell strains. 50,000cells/ 60 mm Petridish were embedded in 0.33% agarose supplemented with media for 2 weeks, colony formation analyzed by DIC microscope. (**C**) Saturation density of HCT116 and its transformed strains analyzed by inoculating 5×10^4 cells/PD_{35} and number of cells/cm^2 area at confluence was measured. (**D**) Proliferation kinetics of exponentially growing HCT116 cell strains. All data is represented as mean ± SE of three independent experiment performed in triplicate

computationally derived and RNAi screens contribute 3% each to the total genes analyzed. Maximum enrichment (162/1066) is depicted in the dataset involving meta-analysis, identifying human genes upregulated in ESCs compared to several differentiated cell types. Moreover, the significance of the enrichment of genes included as transcription factor targets among the input genes found in Stem Checker highlights the maximum overlap with E2F4 followed by SOX2 transcription factor target genes (Fig. 3C).

To further investigate the clinical correlation, we leveraged NCBI-GEO to find a dataset (GSE44076) that closely mimics our cellular model system and corroborate our data with the colorectal cancer tissue dataset. 93 genes were found to be common in transcriptome stem cell expression data and the tissue expression dataset available online, thus validating the involvement of p73 in the stemness of colorectal cancer cells (Fig. 3D).

These observations instigated us to further evaluate the functional CSC features amongst the HCT116 strains. We generated colonospheres in a serum-free defined medium, a technique widely used to study CRC stem cells [16, 17]. The colonosphere initiation was adjusted in such a way that only a single colonosphere was generated in a single well of a 24-well plate. The comparative analysis as a function of time and individual volume of CSC-enriched spheroids indicated varied sphere formation kinetics of all three strains. Despite a comparable initial clustering up to 48 h of all three cell lines, a drastic increase in the volume of colonospheres obtained

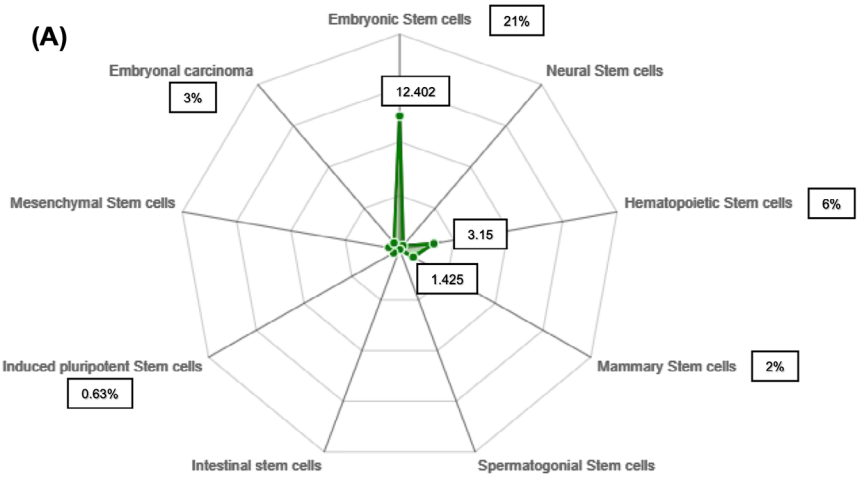

Cell Type	Set Size	Overlapping Genes	Adjusted p value
Embryonic Stem cells	3029	440	3.56E-12
Neural Stem cells	168	20	1.0
Hematopoietic Stem cells	969	135	0.006
Mammary Stem cells	306	43	0.338
Induced pluripotent Stem cells	80	11	1.0
Mesenchymal Stem cells	114	17	0.886
Embryonal carcinoma	653	78	1.0

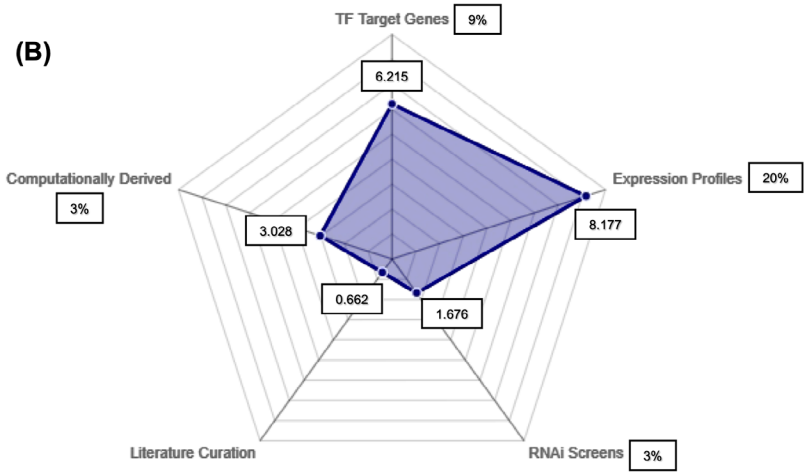

Set Name	Set Size	Overlapping Genes	Adjusted Pvalue
Hs_ESC_Assou	1066	162	4.83E-05
Hs_ESC_SOX2_targets_Boyer	731	114	5.37E-04
GeneCards	133	28	0.009
Hs_ESC_NANOG_targets_Boyer	984	136	0.024
Hs_HSC_Novershtern	854	119	0.037
Hs_ESC_Wong	335	52	0.098
Hs_ESC_Chia	507	69	0.549
Hs_SC_Palmer	184	29	0.551
Hs_ESC_OCT4_targets_Boyer	289	42	0.635
Hs_MaSC_Pece	306	43	0.978
Plurinet	299	41	1

Fig. 3 Enhanced stem cell-like features in HCT116 cell strains: Radar Charts showing the overlap of (**A**) stem cell types (**B**) Stemness Signatures (**C**) Transcription Factors between the list of genes of transcriptome data and Stemchecker database. The overlap significance is plotted as (-log10 p-value) represented by squares on the inner side. Outer squares represent the fractional overlap. The statistical details shown in respective lower panel. The significance (p-value) was calculated by the hypergeometric test and the adjusted p-value is calculated by Bonferroni correction. (**D**) Venn diagram showing the overlap between Transcriptome Stem cell (SC) genes and GSE 44,076 obtained from NCBI-GEO. (**E**) DIC microscopy images of colonosphere of HCT116 strains (magnification 20X) showing progressive increase in size. Colonosphere diameter was measured using NIS-element-AR software was used to calculate the volume of colonospheres (Upper right panel). (**F**) qPCR analysis of EMT associated genes. (**G**) CSC frequency at different time period within the colonosphere of HCT116 strains using flow cytometry. (**H**) DIC images of colonosphere of HCT116 strains (magnification 20X) in float and (**I**) after transferring into tissue culture surface 48 h post attachment

(C)

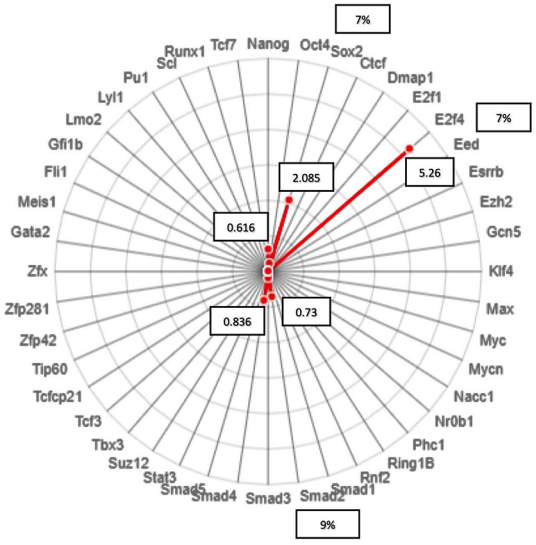

Set Name	Set Size	Overlapping Genes	Adjusted pvalue
Hs_E2F4_Boyer1	1038	156	5.499E-5
Hs_SMAD2_Brown	128	24	0.044
Hs_SMAD3_Brown	128	24	0.044
Hs_SOX2_Boyer1	1156	149	0.082
Hs_SMAD4_Kim	2373	269	1
Hs_NANOG_Boyer1	1511	170	1
Hs_SMAD2_Kim	1619	173	1
Hs_OCT4_Boyer1	566	59	1
Hs_SMAD3_Kim	1266	122	1
Hs_SUZ12_Lee	1509	132	1

(D)

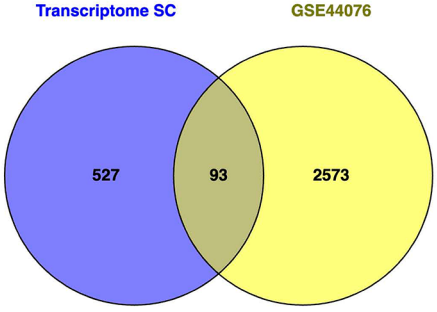

Fig. 3 Continued

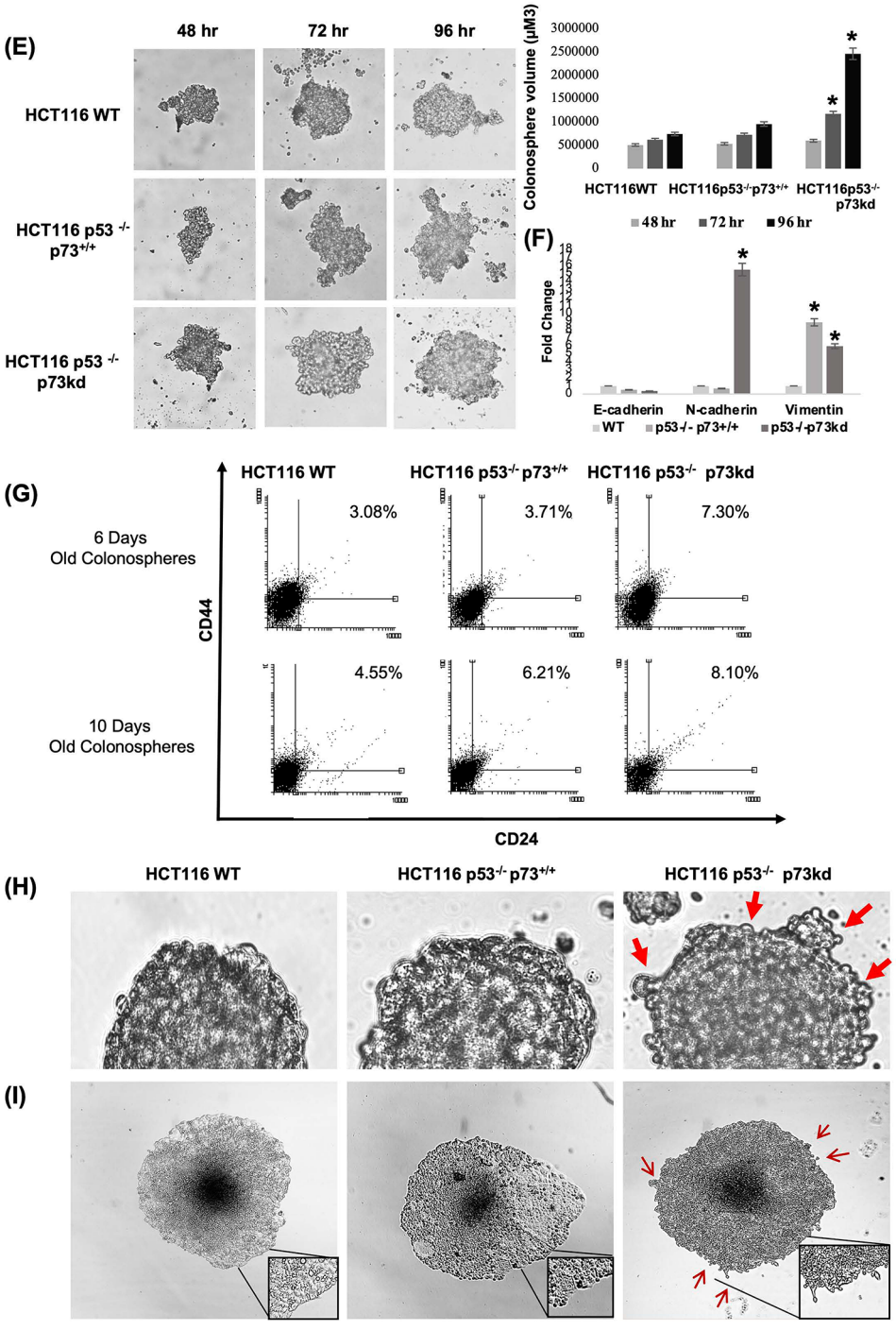

Fig. 3 Continued

by p53-/-p73kd cells was observed up to 96 h of initiation (Fig. 3E). Quite unambiguously, the gene expression profile of EMT-associated genes was also found to be altered in accordance with mesenchymal features of HCT116p53-/-p73kd cells when grown in colonospheres (Fig. 3F). These observations corresponded well with similar EMT genes expression profile observed with 2D cultures of all the strains (Fig. 1E-G).

The functional cancer stem cells (CSC) population majorly reside within $CD24^{+}CD44^{+}$ compartment [18, 19]. Flow cytometric analysis of CD24/CD44 expressing cells revealed a concomitant increase in the CSC frequency with the growth of individual spheroid (Fig. 3G). Remarkably, $p53^{-/-}$p73kd strain exhibited maximum CSC frequency (>50% compared to wt) among all the strains which further found to be increased with the

growth of the spheroids when measured upto 10th day of initiation. The morphology of these free-floating mature spheroids varied remarkably in context to the peripheral margins. Mature colonospheres (>6 days old) of the WT strain displayed a compact arrangement of cells at the periphery, resulting in colonosphere with a smooth surface (Fig. 3H). However, the $p53^{-/-}$p73kd colonospheres explicitly displayed cells extending out from the peripheral region of colonospheres. These cellular extensions could be observed in routine examinations and persisted until the disintegration of the spheroids at later time points (data not shown). To rule out the possibility of any artifact, colonospheres were placed onto a tissue culture plastic plate resulting in outward cellular migration on the surface. We observed distinct single cells with directional movement and protruding lamellipodia in the $p53^{-/-}$p73kd strain (Fig. 3I (20X)/inset) while the two preceding strains could not show this phenomenon.

Based on the comprehensive analysis of various markers and functional characteristics, these cells exhibit stem cell-like properties. This suggests that further detailed functional studies could be conducted to confirm their stemness.

Esculetin suppresses the aggressive behavior of HCT116 strains without inducing marked cytotoxicity

We previously demonstrated the antiproliferative effects of esculetin in AML and pancreatic cancer cells, and its ability to induce neutrophilic differentiation in leukemic blast cells [7, 8, 20] Therefore, to evaluate effect of esculetin in our current cellular model, we examined the cytotoxic effect. cells were treated with esculetin for up to 48 h at different concentrations (0-500 µM) and subjected to MTT assay (Fig. 4A). We observed an insignificant cytotoxicity in all of the three strains up to 500µM of esculetin. The IC_{50} could not be however, calculated due to inadequate cell death even at the highest concentration used i.e. 500µM. In contrast, a marked reduction in proliferation potential was observed in esculetin-treated cell strains (Fig. 4B). It is important to note that the cell proliferation was considerably suppressed within 24 h of 100µM esculetin treatment with no marked cell death (Fig. 4A and B). Since at 100µM concentration, esculetin could inhibit the growth, all further assays were carried out on HCT116 cell strains at 100µM concentration of esculetin with appropriate controls. The growth suppressive effect of esculetin was further substantiated by aberrant cell cycle distribution analyzed at varied time intervals following 100 µM esculetin treatment. Esculetin treated cells of all the three strains displayed a comparable cell cycle distribution where a concomitant increase in the proportion of G1/S phase cells while a reduction in cells in G2/M phase were observed (Fig. 4C). The G1/S arrest was more prominent at 24 h following esculetin treatment.

The potential of esculetin to affect additional aggressive phenotypes such as the migratory capacity and anoikis resistance were also assessed. While the three cell strains inherently exhibit a sequentially higher migratory potential, we found a significant (~60%) reduction in cell migration in cells with partial ($p53^{-/-}p73^{+/+}$) or complete ($p53^{-/-}$p73kd) mesenchymal features (Fig. 4D/supplementary Fig. 2) upon esculetin treatment. Reduction in cell migration was accompanied by a drastic reduction (>80%) in anoikis resistance in these two strains (Fig. 4E).

Reversion of stem cell like features and concurrent EMT phenotypes upon esculetin exposure

We further evaluated effects of esculetin on the plasticity of cells with prominent mesenchymal features i.e., HCT116p53-/-p73kd.

A remarkable conversion of elongated spindle shaped cells into relatively cobblestone-like morphology was evidently observed in esculetin-treated cells during exponential phase of the culture (Fig. 5A). On the other hand, HCT116WT and HCT116$p53^{-/-}p73^{++}$ showed the similar response at a much lower extent (Supplementary Fig. 3). Despite the inherent epithelial-mesenchymal transition (EMT) characteristics among the three cell lines, the effect of esculetin was more pronounced in HCT116p53-/-p73-/- cells, likely due to their inherently higher mesenchymal characteristics. Esculetin was also found to upregulate E-cadherin expression levels in the p53 deletion strains while N-cadherin reduction was more profound in the $p53^{-/-}$p73kd cells (Fig. 5B). Coincidently, esculetin markedly abolished the colony growth in methylcellulose media suggesting the suppressive effects of esculetin on the clonogenic ability of cells (Fig. 5C). Cells exposed to esculetin significantly suppressed the expression levels of transcription factors such as *SNAIL1*, *TWIST1*, *and ZEB2* (Fig. 5D). Cells protruding out from the growing spheroids also depleted drastically upon esculetin treatment (Fig. 5E) leading to colonosphere morphology comparable to that of the WT strain. We also observed that esculetin reduced the stem cell population as evidenced by reduced $CD24^{+}/CD44^{+}$ population when analyzed by flowcytometry (Fig. 5F). CSCs with $CD90^{+}$ phenotypes have been explicitly identified in verity of tumor types making CD90 an attractive therapeutic target [21]. We detected ~two-fold reduction in $CD90^{+}$ population within colonospheres upon esculetin exposure (Fig. 5G). These observations clearly indicated the potential of esculetin to reduce the CSC population and concurrent EMT reprogramming in cells with mesenchymal features.

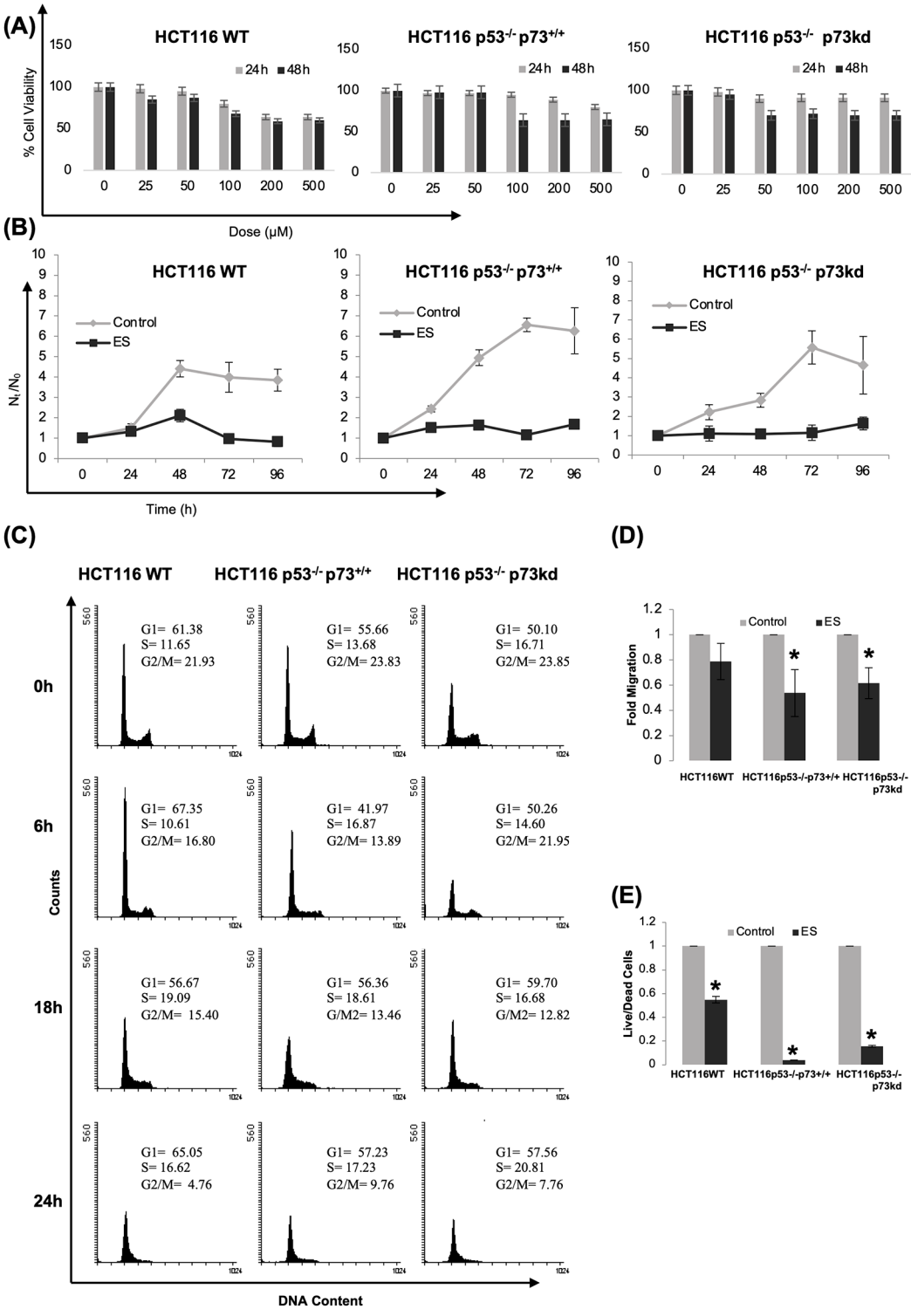

Fig. 4 Suppression of cell aggressiveness by esculetin: (**A**) Dose response bar plot of MTT assay to measure the effect of varied concentration of esculetin on cell viability of HCT116 cell strains. (**B**) Cell proliferation kinetics assessed with and without 100μM esculetin treatment. Data is represented as mean ± SE of three independent experiment performed in triplicate. (**C**) Cell cycle analysis of HCT116 cell strains following 100 μM esculetin treatment using flow cytometry at indicated time intervals. (**D**) Analysis of wound healing assay following 100μM esculetin treatment for 18-hour post seeding. (**E**) Anoikis resistance measured by counting floating dead cells 48 h post 100μM esculetin treatment. All Data is represented as mean ± SE of one experiment performed in triplicate (*$p \leq 0.05$ & **$p \leq 0.01$)

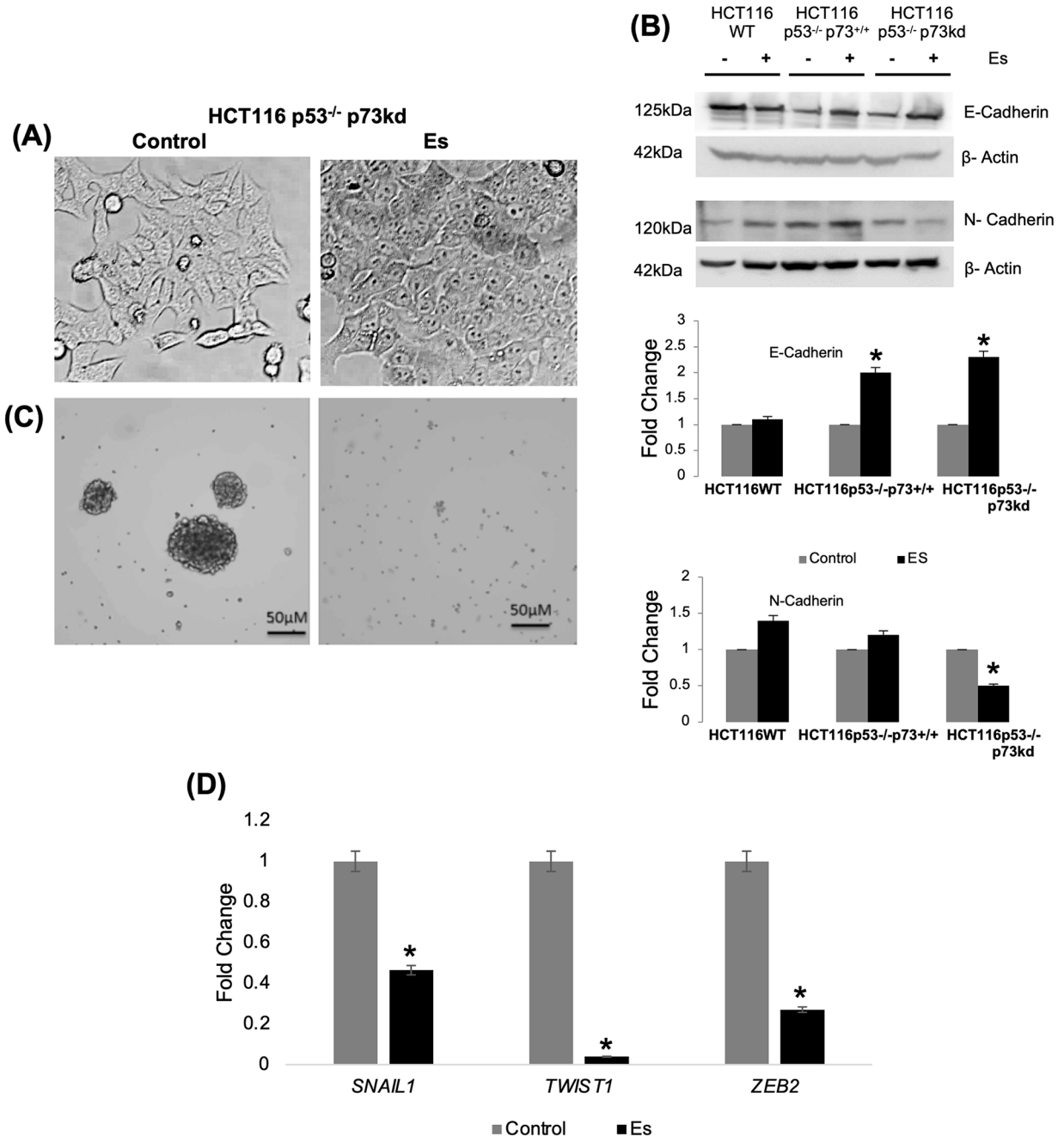

Fig. 5 Reversion of EMT and stem cell-like characteristics upon esculetin treatment: (**A**) DIC photomicrograph of cells showing reversion of mesenchymal phenotype at 72 h following 100μM esculetin treatment. (**B**) Western blot analysis of expression of E-cadherin and N-cadherin protein isolated from control and esculetin treated cells after 48 h of 100μM esculetin treatment. Representative histogram plot of densitometic analysis of protein expression relative to β-actin expression (*$p \leq 0.05$ & **$p \leq 0.01$). (**C**) Colonosphere growth in CSC media containing 1% methylcellulose to assess clonogenic ability of cells. (**D**) qRT-PCR analysis of key transcription factors (**E**) DIC images of single (left panel/magnification 63X) and multiple (right panel/magnification 20X) colonospheres growth with/without 100μM esculetin treatment. (**F**) Flow cytometric analysis of HCT116p53$^{-/-}$p73kd cells treated with/without esculetin to measure CSC frequency in CD24+/CD44 + compartment. (**G**) Cell surface expression analysis of CD90 using flow cytometry following 96 h of esculetin treatment. Percentage of shifted cells was measured using flowing software. Data represents at least three independent experiment performed in triplicates

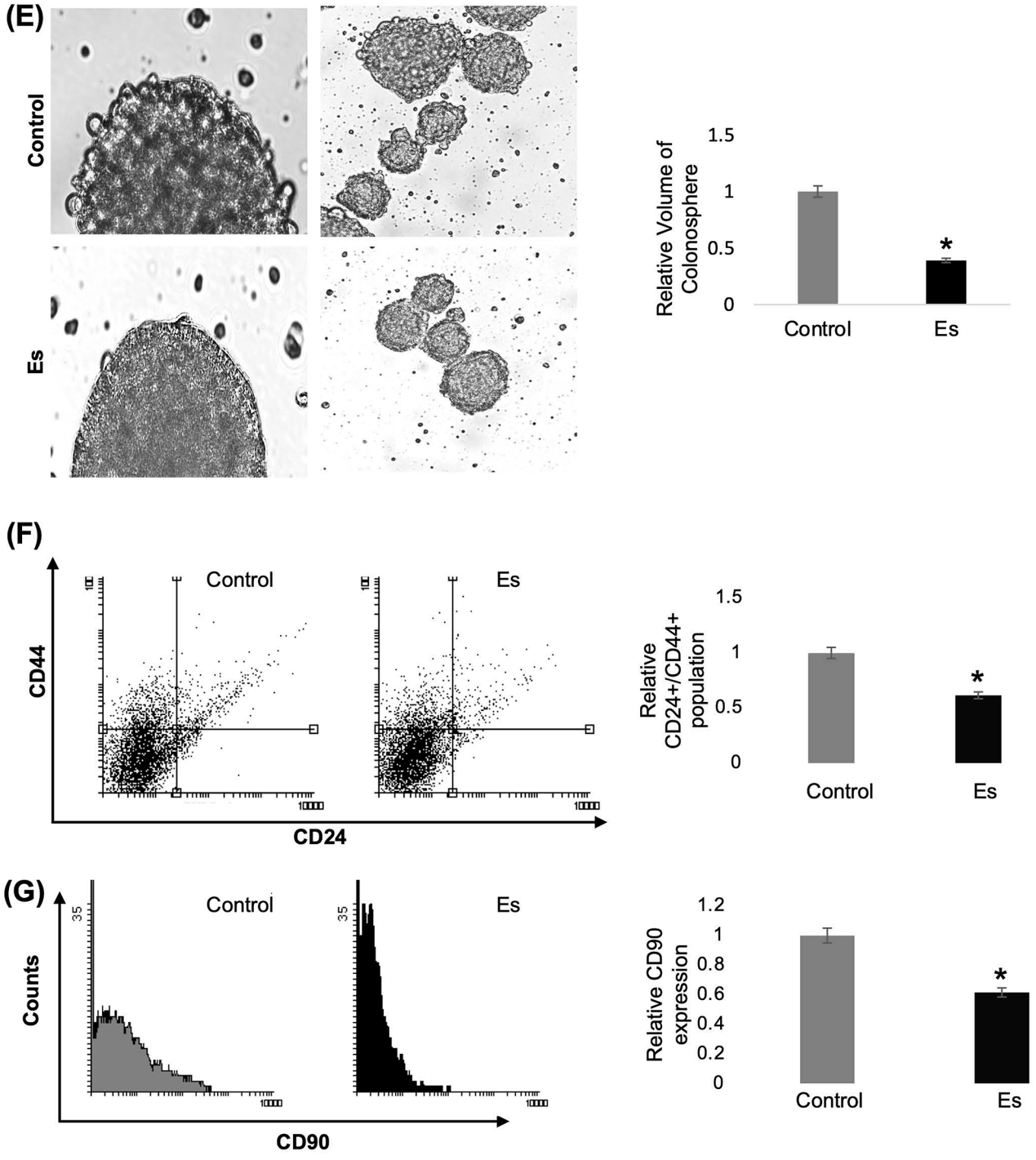

Fig. 5 Continued

Esculetin induces differentiation in stem cells with high mesenchymal characteristics and "axis shift "of wnt signaling

We further extended our investigation by analysing the stemness-associated genes in esculetin treated/untreated cells. POU class 5 homeobox 1 (*POU5F1/OCT4*) and Aldehyde Dehydrogenase 1(*ALDH1*) are well-studied genes associated with stemness maintenance were found to be drastically suppressed upon esculetin exposure (Fig. 6A). The esculetin treatment resulted in a decrease in stemness markers in treated cells, concomitant with a remarkable (up to five-fold) augmentation in colonic

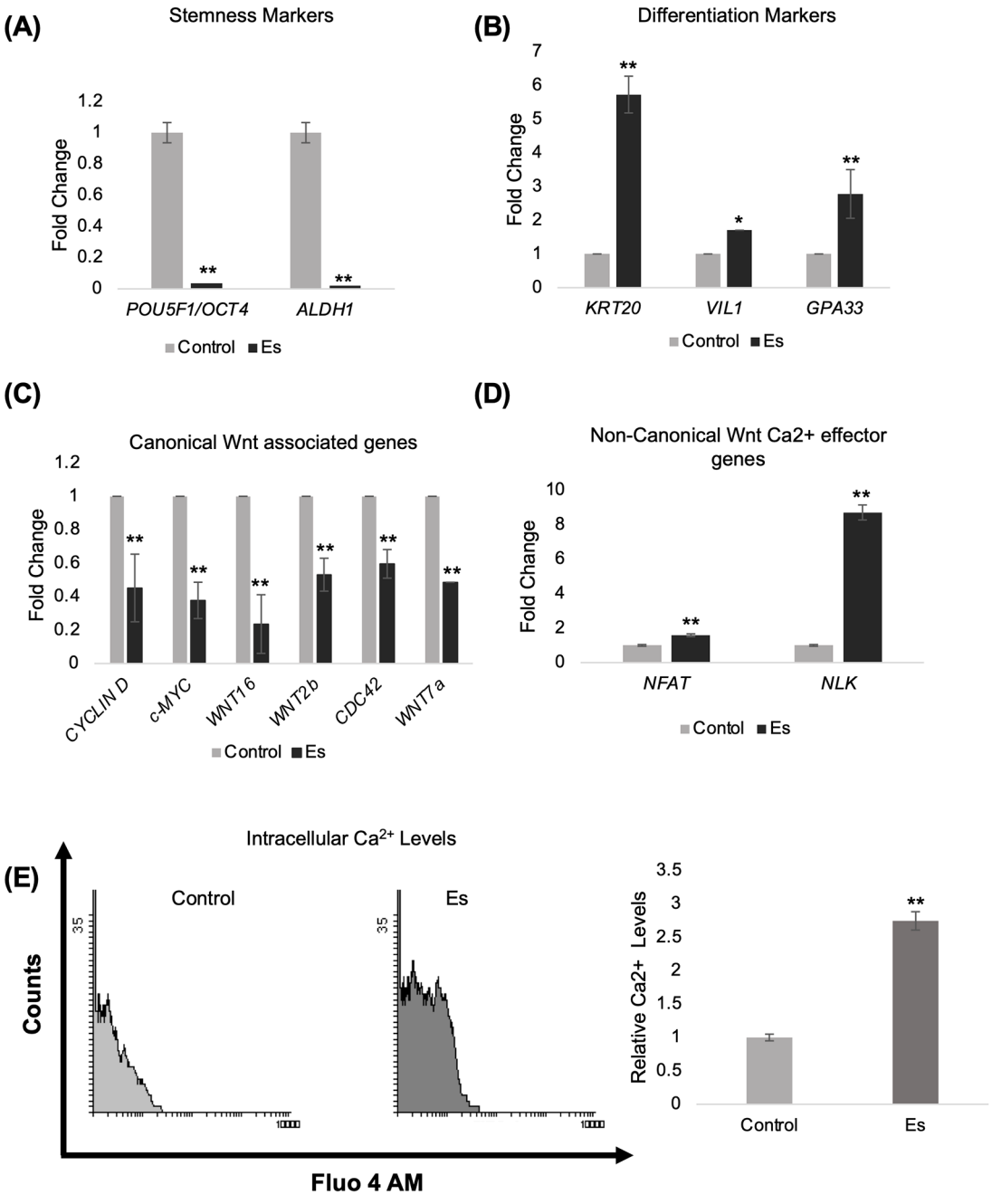

Fig. 6 Wnt axis shift during esculetin mediated differentiation: qPCR analysis to check the expression level of indicated stemness (**A**) and differentiation (**B**) marker genes. Data represents three independent experiments. Expression levels of genes associated with canonical (**C**) and non-canonical Wnt $Ca2^{+}$ pathway (**D**) were analysed by qPCR. (**E**) Analysis of intracellular calcium levels following 72 h esculetin treatment. Cells were harvested and stained with intracellular calcium binding dye -Fluo-4AM and analysed using flow cytometry. Relative fold change to untreated cells was plotted (right panel). (*$p \leq 0.05$ & **$p \leq 0.01$)

differentiation markers (*KRT20, VIL1, and GPA33*), which are recognized for their elevated expression in colonic epithelium (Fig. 6B).

The Wnt signaling plays a central cascade in regulating stemness features. We found a significant downregulation of signaling components associated with canonical Wnt axis (*CYCLIN D*, *c-MYC*, *Wnt16*, *Wnt2b*, *CDC42*, *WNT7a*) (Fig. 6C) while upto eight-fold increase in non-canonical Ca^{2+} effector genes (*NFAT*, *NLK*) (Fig. 6D) upon esculetin treatment. These observations suggest that esculetin regulates CSC differentiation by switching Wnt cascade from

canonical to non-canonical Ca^{2+} axis. Activation of non-canonical Ca^{2+} axis was further supported by enhanced intracellular Ca^{2+} levels when analysed with FACS (Fig. 6E).

Suppression of non-canonical Wnt/Ca^{+2} axis abrogates esculetin mediated CSC differentiation

To further validate the involvement of non-canonical Wnt axis in esculetin mediated differentiation in CSCs, we abrogated the non-canonical Wnt axis by inhibiting the intracellular Ca^{+2} levels using calcium channel blocker TBM8. Inhibiting the ER-IPR channels by TMB8 resulted in drastic reduction in intracellular Ca^{+2} levels (Fig. 7A). Quite remarkably, inhibition of intracellular Ca^{+2} levels significantly suppressed esculetin mediated differentiation in $p53^{-/-}$p73kd cells (Fig. 7B) as indicated by up to 3-fold downregulation of differentiation-associated genes (KRT20 GPA33). Interestingly, up to a four-fold increase in stemness markers (*POU5F1/OCT4 and ALDH1*) expression levels in Es+TMB8 cells was also

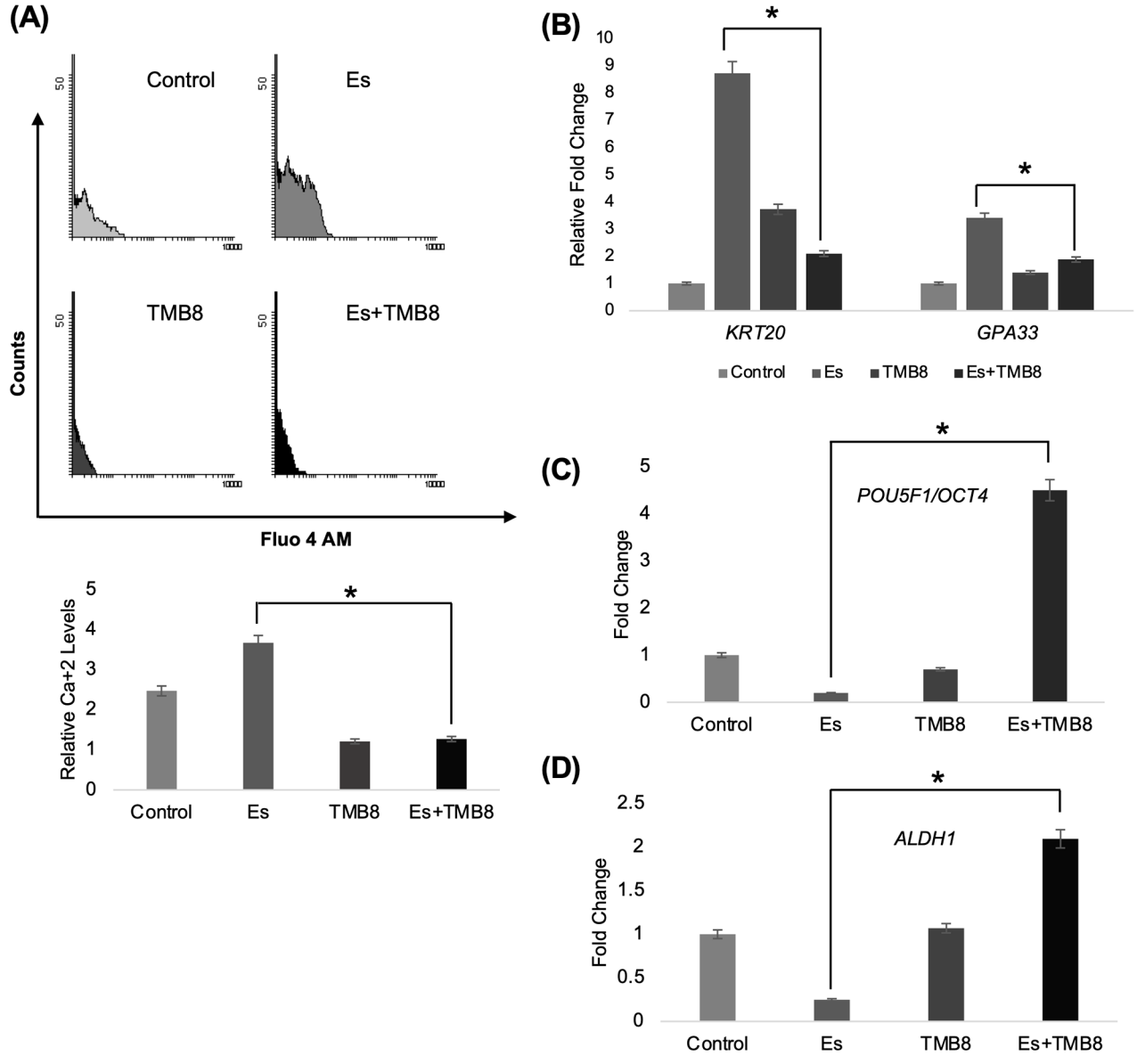

Fig. 7 Involvement of Non-canonical Wnt Ca^{2+} pathway in CSC differentiation: (**A**) Flow cytometric analysis of effect of TMB8 (calcium channel blocker) on intracellular calcium levels. Cells were treated with esculetin alone or in combination with TMB8 for 72 h and stained with Fluo-4AM. A right shift in the fluorescence intensity demonstrate enhanced intracellular calcium levels in response to esculetin treatment. Relative fold change of three independent experiments performed in triplicates were shown in lower panel. (*$p \leq 0.05$). (**B**) qPCR analysis of colonic differentiation markers KRT20, GPA33 and stemness markers (**C**) *POU5F1/OCT4* (**D**) *ALDH1*in cells treated with esculetin alone or in combination with TMB8 for 96 h

observed (Fig. 7C and D). These results strongly suggest essential role of non-canonical Wnt activation in esculetin-mediated CSC differentiation. These findings strongly indicate the crucial involvement of non-canonical Wnt activation in esculetin-induced differentiation of cancer stem cells.

Discussion

EMT is an integral process of tissue repair and development and also known to contribute in pathological processes such as fibrosis and cancer progression [22]. Considering the heterogeneity of disseminating cancer cells, EMT is proposed to be a graded series of interplaying events that promote unstable genetic environment. Some distinctions of EMT induction result from gain of functions in oncogenes and inactivation of tumour suppressor genes in the transforming cells [23]. In the current study, we report the interrogation of sequential knockdown of p53/p73 to generate phenotypically distinct strains of HCT116 cells which simulate EMT reprogramming and CSC characteristics. The majority of the studies on EMT are based on artificial induction of EMT using variety of inducers [24, 25]. Herein, we demonstrate inherent EMT induction as well as concurrent acquisition of stem cell features as a result of knockdown of p53/p73 genes. Further, we evaluated the efficacy of esculetin to affect the inter-conversion of epithelial to mesenchymal phenotype inherited with stem cell-like characteristics. Quite importantly, our study suggests that p53/p73 are associated with the maintenance of cellular plasticity, deletion of one and/or another gene corresponds with acquisition of aggressive behavior in transforming cells.

P53 is a well-established tumour suppressor gene that regulates various cellular processes in response to stress signals [26, 27]. However, recent studies have highlighted the relative importance of p53 in modulating other cellular processes apart from canonical p53-mediated tumour suppression viz. metabolism, cellular plasticity, invasion and metastasis. For example; p53 knockdown have been shown to induce EMT and stemness property through miRNAs in hepatocellular carcinoma and mammary epithelial cells [28, 29] as well as enhancement in TGF-β induced EMT in hepatocellular carcinoma [25]. In agreement with these studies, we demonstrate the role of p53 in maintaining cellular plasticity in CRC. In parallel to the increasing knowledge of p53 dynamics, several crucial issues remain unanswered for the biological role of its recently identified family protein p73. In the present study, knockdown of p73 gene in p53 null cell strain, further heighten the aggressiveness in HCT116p53$^{-/-}$p73kd cells as evident by enhanced mesenchymal characteristics akin to stem cell transformation. However, these cells showed limited capacity to gain anchorage independency and tumorigenic potential. Accumulated evidences suggests that cancer cells with stem cell-like features exhibit mesenchymal features associated with invasion and metastasis. In accordance, our study further highlights that stemness and EMT regulatory mechanisms are integrally associated to drive invasive events as indicated by induction of pluripotent stem cell features in cells with prominent mesenchymal features when analyzed by integrative bioinformatics as well as functional approaches. In continuation with recently identified epigenetic and microenvironmental regulatory mechanisms, we propose that "axis shift" of the Wnt pathway plays a central role in coordinating EMT and stem cell-like characteristics in cancer cells. Recently, targeting CSC differentiation by regulating specific signaling pathways has been emerging to achieve complete remission of the disease which have shown to generate robust therapeutic response in preclinical models of solid tumours. For example, induction of differentiation in hepatocellular carcinoma cells prevents tumour growth in mice [30] while exposure to anti-R-Spondin 3 antibody suppressed tumour growth and stemness by inducing CSC differentiation [31]. In the current study, we demonstrate that esculetin at 100 μM concentration markedly induces enterocyte differentiation and epithelial cell polarity in CSCs of cells with high mesenchymal features. These observations corroborated our findings with leukemic blast cells posing esculetin as a differentiating agent in both AML as well as solid tumour cells. Moreover, esculetin significantly suppressed the EMT reprogramming regulating CSC phenotype in HCT116 cells with p53/p73 knockdown as indicated by reduced anchorage independency, migration, and anoikis resistance. Inhibition of the aggressive behavior with esculetin treatment was accompanied by reduced EMT phenotype and marker expressions. In addition, esculetin have been shown to induce differential G1/S phase cell cycle arrest in cells with varying p53/p73 status. These observations may introduce esculetin as a potent natural compound to reinforce the chemotherapeutics of advanced stage cancers. Since in the present study, esculetin have shown inhibitory action rather than a marked cytotoxicity in the colorectal cancer undergoing EMT, it may be proposed for a combination therapy along with a potent conventional/natural cytotoxic agent. Taken together, our data indicate an interventional effect of esculetin on EMT and stem cell-like characteristics of high-grade tumours.

We recognize that, despite extensive analyses encompassing CSC marker profiling, transcriptomic assessments, and various functional assays, the functional attributes of CSCs require further investigation. Our current study suggests that the CD24^{+}CD44^{+} subpopulation within our colorectal cancer cell line exhibits characteristics consistent with stem cell-like properties. Findings highlighting stemness and

self-renewal properties encourage us to pursue these investigations in future studies.

In summary, this study demonstrates the intricate association of p53/p73 with the acquisition of EMT characteristics and concurrent stem cell-like features in HCT116 cells. Successive deletion of these genes may predispose a transforming cell to invade the primary site. Interestingly, esculetin attenuates the aggressive mesenchymal features and stemness of colon carcinoma cells by reversing EMT phenotypes. The current findings, in accordance with our previous observations with leukemic cells may open an exploitable window for esculetin to consider as a potent differentiating agent in both leukemic as well as solid tumours.

Supplementary Information

The online version contains supplementary material available at https://doi.org/10.1186/s12885-024-12736-2.

Supplementary Material 1

Supplementary Material 2

Supplementary Material 3

Supplementary Material 4

Supplementary Material 5

Acknowledgements
The authors thank the financial support from ACBR and IoE grant to DS. The Research Associate fellowship and contingency grant from Department of Biotechnology (DBT) and Maharishi Kanad post-doctoral fellowship (University of Delhi) to AM is highly acknowledged.

Author contributions
DS and AM conceived the project and wrote the manuscript. AM performed all the experiments. Data curation and analysis was performed by DS, AM and CB. MM and AS performed real time PCR, and helped in flow cytometry experiments. DS supervised throughout the study. All authors have read and approved the final manuscript.

Funding
DS received funding from ACBR and Institution of Eminence (No./IoE/2021/12/FRP), University of Delhi. AM received his post-doctoral fellowship and contingent grant from Department of Biotechnology, Govt. of India (DBT-RA/Batch 34/AM) and Institute of Eminence (IoE/2021/MKPDF/DSPH/178), University of Delhi.

Data availability
The datasets used and/or analysed during the current study available from the corresponding author on reasonable request.

Declarations

Ethics approval and consent to participate
Not applicable.

Consent for publication
Not applicable.

Competing interests
The authors declare no competing interests.

Received: 8 February 2024 / Accepted: 30 July 2024
Published online: 19 September 2024

References

1. Jolly MK, Celià-Terrassa T. Dynamics of Phenotypic Heterogeneity Associated with EMT and stemness during Cancer Progression. J Clin Med. 2019;8(10):1542. https://doi.org/10.3390/jcm8101542.
2. Mathur A, Chinnadurai V, Bhalla PJS, Chandna S. Induction of epithelial-mesenchymal transition in thyroid follicular cells is associated with cell adhesion alterations and low-dose hyper-radiosensitivity. TUB. 2023;45(1):95–110. https://doi.org/10.3233/TUB-220027.
3. Tang DG. Understanding cancer stem cell heterogeneity and plasticity. Cell Res. 2012;22(3):457–72. https://doi.org/10.1038/cr.2012.13.
4. Yang L, Shi P, Zhao G, et al. Targeting cancer stem cell pathways for cancer therapy. Sig Transduct Target Ther. 2020;5(1):8. https://doi.org/10.1038/s41392-020-0110-5.
5. Shi ZD, Pang K, Wu ZX, et al. Tumor cell plasticity in targeted therapy-induced resistance: mechanisms and new strategies. Sig Transduct Target Ther. 2023;8(1):113. https://doi.org/10.1038/s41392-023-01383-x.
6. Van Gils N, Verhagen HJMP, Smit L. Reprogramming acute myeloid leukemia into sensitivity for retinoic-acid-driven differentiation. Exp Hematol. 2017;52:12–23. https://doi.org/10.1016/j.exphem.2017.04.007.
7. Sawney S, Arora R, Aggarwal KK, Saluja D. Esculetin Downregulates the expression of AML1-ETO and C-Kit in Kasumi-1 cell line by decreasing half-life of mRNA. J Oncol. 2015;2015:1–8. https://doi.org/10.1155/2015/781473.
8. Mathur A, Gangwar A, Saluja D. Esculetin releases maturation arrest and induces terminal differentiation in leukemic blast cells by altering the wnt signaling axes. BMC Cancer. 2023;23(1):387. https://doi.org/10.1186/s12885-023-10818-1.
9. Uboveja A, Satija YK, Siraj F, Saluja D. p73-regulated FER1L4 lncRNA sponges the oncogenic potential of miR-1273 g-3p and aids in the suppression of colorectal cancer metastasis. iScience. 2022;25(2):103811. https://doi.org/10.1016/j.isci.2022.103811.
10. Yang D, Louden C, Reinhold DS, Kohler SK, Maher VM, McCormick JJ. Malignant transformation of human fibroblast cell strain MSU-1.1 by (+-)-7 beta,8 alpha-dihydroxy-9 alpha,10 alpha-epoxy-7,8,9,10-tetrahydrobenzo [a]pyrene. Proc Natl Acad Sci U S A. 1992;89(6):2237–41. https://doi.org/10.1073/pnas.89.6.2237.
11. Liu S, Dontu G, Mantle ID, et al. Hedgehog signaling and Bmi-1 regulate self-renewal of normal and malignant human mammary stem cells. Cancer Res. 2006;66(12):6063–71. https://doi.org/10.1158/0008-5472.CAN-06-0054.
12. Mathur A, Kumar A, Babu B, Chandna S. In vitro mesenchymal-epithelial transition in NIH3T3 fibroblasts results in onset of low-dose radiation hypersensitivity coupled with attenuated connexin-43 response. Biochim Biophys Acta Gen Subj. 2018;1862(3):414–26. https://doi.org/10.1016/j.bbagen.2017.11.013.
13. Wang Y, Chen X, Cao W, Shi Y. Plasticity of mesenchymal stem cells in immunomodulation: pathological and therapeutic implications. Nat Immunol. 2014;15(11):1009–16. https://doi.org/10.1038/ni.3002.
14. Kasamaki A, Yasuhara T, Urasawa S. Neoplastic transformation of Chinese hamster cells in vitro after treatment with flavoring agents. J Toxicol Sci. 1987;12(4):383–96. https://doi.org/10.2131/jts.12.383.
15. Rubin H. Degrees and kinds of selection in spontaneous neoplastic transformation: an operational analysis. Proc Natl Acad Sci U S A. 2005;102(26):9276–81. https://doi.org/10.1073/pnas.0503688102.
16. Gheytanchi E, Naseri M, Karimi-Busheri F, et al. Morphological and molecular characteristics of spheroid formation in HT-29 and Caco-2 colorectal cancer cell lines. Cancer Cell Int. 2021;21(1):204. https://doi.org/10.1186/s12935-021-01898-9.
17. Olejniczak A, Szaryńska M, Kmieć Z. In vitro characterization of spheres derived from colorectal cancer cell lines. Int J Oncol Published Online November. 2017;16. https://doi.org/10.3892/ijo.2017.4206.
18. Vaiopoulos AG, Kostakis ID, Koutsilieris M, Papavassiliou AG. Colorectal Cancer stem cells. Stem Cells. 2012;30(3):363–71. https://doi.org/10.1002/stem.1031.
19. Yeung TM, Gandhi SC, Wilding JL, Muschel R, Bodmer WF. Cancer stem cells from colorectal cancer-derived cell lines. Proc Natl Acad Sci USA. 2010;107(8):3722–7. https://doi.org/10.1073/pnas.0915135107.
20. Arora R, Sawney S, Saini V, Steffi C, Tiwari M, Saluja D. Esculetin induces antiproliferative and apoptotic response in pancreatic cancer cells by directly

binding to KEAP1. Mol Cancer. 2016;15(1):64. https://doi.org/10.1186/s12943-016-0550-2.
21. Shaikh MV, Kala M, Nivsarkar M. CD90 a potential cancer stem cell marker and a therapeutic target. CBM. 2016;16(3):301–7. https://doi.org/10.3233/CBM-160590.
22. Kalluri R. When epithelial cells decide to become mesenchymal-like cells. J Clin Invest. 2009;119(6):1417–9. https://doi.org/10.1172/JCI39675.
23. Lee EYHP, Muller WJ. Oncogenes and tumor suppressor genes. Cold Spring Harb Perspect Biol. 2010;2(10):a003236. https://doi.org/10.1101/cshperspect.a003236.
24. Pang MF, Georgoudaki AM, Lambut L, et al. TGF-β1-induced EMT promotes targeted migration of breast cancer cells through the lymphatic system by the activation of CCR7/CCL21-mediated chemotaxis. Oncogene. 2016;35(6):748–60. https://doi.org/10.1038/onc.2015.133.
25. Wang Z, Jiang Y, Guan D et al. Critical Roles of p53 in Epithelial-Mesenchymal Transition and Metastasis of Hepatocellular Carcinoma Cells. Syn WK, ed. *PLoS ONE*. 2013;8(9):e72846. https://doi.org/10.1371/journal.pone.0072846
26. Bieging KT, Mello SS, Attardi LD. Unravelling mechanisms of p53-mediated tumour suppression. Nat Rev Cancer. 2014;14(5):359–70. https://doi.org/10.1038/nrc3711.
27. Steele RJC, Thompson AM, Hall PA, Lane DP. The *p53* tumour suppressor gene. Br J Surg. 2003;85(11):1460–7. https://doi.org/10.1046/j.1365-2168.1998.00910.x.
28. Chang CJ, Chao CH, Xia W, et al. p53 regulates epithelial–mesenchymal transition and stem cell properties through modulating miRNAs. Nat Cell Biol. 2011;13(3):317–23. https://doi.org/10.1038/ncb2173.
29. Kim T, Veronese A, Pichiorri F, et al. p53 regulates epithelial–mesenchymal transition through microRNAs targeting ZEB1 and ZEB2. J Exp Med. 2011;208(5):875–83. https://doi.org/10.1084/jem.20110235.
30. Jiao J, González Á, Stevenson HL, et al. Depletion of S100A4 + stromal cells does not prevent HCC development but reduces the stem cell-like phenotype of the tumors. Exp Mol Med. 2018;50(1):e422–422. https://doi.org/10.1038/emm.2017.175.
31. Storm EE, Durinck S, De Sousa E, Melo F, et al. Targeting PTPRK-RSPO3 colon tumours promotes differentiation and loss of stem-cell function. Nature. 2016;529(7584):97–100. https://doi.org/10.1038/nature16466.

Publisher's Note